Scanning Microscopy

Volume 1 | Number 1 Article 4

12-10-1986

Magnetic Domain Observation using Spin-Polarized Scanning Electron Microscopy

K. Koike
Hitachi, Ltd.

H. Matsuyama
Hitachi, Ltd.

H. Todokoro
Hitachi, Ltd.

K. Hayakawa
Hitachi, Ltd.

Scanning Microscopy, Vol. 1, No. 1, 1987 (Pages 31-39) 0981-7035/87$3.00+.00
Scanning Microscopy International, Chicago (AMF O'Hare), IL 60666 USA

MAGNETIC DOMAIN OBSERVATION USING SPIN-POLARIZED SCANNING ELECTRON MICROSCOPY

K. Koike,† H. Matsuyama, H. Todokoro,* and K. Hayakawa

Advanced Research Laboratory, Hitachi, Ltd., Kokubunji, Tokyo 185, Japan
*Central Research Laboratory, Hitachi, Ltd., Kokubunji, Tokyo 185, Japan

(Received for publication February 12, 1986, and in revised form December 10, 1986)

Abstract

A new apparatus, spin-polarized scanning electron microscope (SEM), has been developed. This is a unique apparatus, which forms images by electron spin polarization. By using this device, magnetic domain images can be obtained because secondary electrons from ferromagnetic samples are polarized representing the magnetization of the sample originating point. This method provides new capabilities, such as magnetic contrast independent of surface morphology, detection of magnetization direction, and high spatial resolution.

Key Words: Spin, polarization, Mott detector, magnetic domain.

†Address for correspondence:
K. Koike
Advanced Research Laboratory
Hitachi, Ltd., Kokubunji, Tokyo 185
Japan
Phone No. 0423-23-1111

Introduction

In conventional electron microscopes, the intensity of the electron beam (number of electrons) from a sample has played an important role in producing image contrasts. In addition to the intensity, this electron beam has another quantitatively measurable characteristic, spin polarization. However, spin polarization has long been neglected in electron microscopes because its detection is complex, so that the identification of polarized electrons from a sample is difficult.

Towards the end of the 1960's, the study of spin polarization of electrons emitted from or scattered by solids began. Since that time, various electrons have been found to be polarized. Polarized secondary electrons from a ferromagnetic sample is one such finding (Chrobok and Hofmann, 1976). The polarization of these electrons was suggested for use in scanning electron microscopes (SEMs) in order to observe magnetic domains (DiStefano, 1978, Unguris et al., 1982, Kirschner, 1984). Recently, this new domain observation method has been realized (Koike and Hayakawa, 1984a) and is referred to as spin-polarized scanning electron microscopy.

There are various methods for observing magnetic domains. These methods include the Bitter method, optical microscopy (using the Kerr or Faraday effects), Lorentz microscopy, scanning electron microscopy (using the deflection of secondary electrons near the sample surface (Type I) or the deflection of scattered electrons inside the sample (Type II)) and electron holography.

Compared to these conventional methods, spin-polarized scanning electron microscopy has new capabilities, such as high spatial resolution even for thick samples (Koike et al., 1985c), magnetic contrast independent of surface morphology (Koike and Hayakawa, 1984b) and magnetization direction detection. This paper reviews this novel magnetic domain observation method, and provides additional data for its use.

Principles of Magnetic Domain Observation

Polarization of secondary electrons from ferromagnetic samples

Various studies have been conducted since Chrobok and Hofmann (1976) found that secondary electrons from a ferromagnetic sample are polarized representing sample magnetization. The relationship between polarization and the energy of electron-excited secondary electrons from nickel is shown in Figure 1 (Hopster et al., 1983). At energies above 6eV, the polarization

is almost constant and is the same as 5.5% d-band polarization. With a decrease in energy, polarization increases and reaches a maximum of 17% at zero energy. This feature is explained as follows.

Secondary electrons with higher energies are directly excited from the d-band by primary electrons, and inherit d-band polarization. On the other hand, those with lower energies are produced by a cascade process where spin-dependent inelastic scattering enhances the spin polarization so that it is much larger than that of the d-band (Hopster et al., 1983, Penn et al., 1985a,b). Similar results were obtained with photon-excited secondary electrons from iron and cobalt (Kisker et al., 1982).

Since the electronic charge sign is negative, the angular momentum of electrons is antiparallel to the magnetic moment. Therefore, the polarization vector defined in terms of the angular momentum is antiparallel to the magnetization vector whose origin is the electron magnetic moment.

Polarization measurement

Various methods have been reported for detecting electron spin polarization, such as the polarized low-energy electron diffraction detector (Kirschner and Feder, 1979), absorption current detector (Siegmann et al., 1981) and Mott detector. Among these, the Mott detector is generally used because of its reliable past performance, stability, and relatively high efficiency. Since the Mott detector is also used in spin-polarized scanning electron microscopy, it is briefly described here.

The basic principle of the Mott detector is shown in Figure 2. Polarized high energy electrons moving towards the heavy atom film are scattered by it. In this case, the number of electrons scattered into two symmetrical right-left directions are not equal because of spin orbit interaction. If these numbers are defined as N_r and N_l, the polarization vector component P_i, normal to the scattering plane, is determined by:

$$P_i = (1/S)(N_l - N_r) / (N_l + N_r) \quad (1)$$

where S is a constant determined by the scattering condition only.

Principles and Capabilities of Domain Observation

Principles

The principles of magnetic domain observation using spin-polarized scanning electron microscopy are shown in Figure 3. As mentioned above, the polarization vector of secondary electrons from the ferromagnetic substance is antiparallel to the magnetization vector at the originating point on the sample. Consequently, a magnetic domain image can be formed if the sample surface is scanned by a fine primary electron beam, and if P_i of the generated secondary electrons is detected and used as an SEM image signal. This method has new capabilities not included in more conventional techniques. These capabilities are now presented.

High Spatial Resolution

Spatial resolution of this method is determined by the probe diameter of the primary electron beam. However, the efficiency of the polarization detector is extremely low compared with that of a simple electron detector which detects electron number or beam intensity. As a result, noise due to statistical errors in the detected polarization increases and image quality deteriorates. Therefore, a much larger probe current is needed in a spin-polarized SEM than in an ordinary SEM to maintain a good image signal to noise ratio.

The statistical error δP_i of the measured polarization P_i is expressed by:

$$\delta P_i = \sqrt{(1/N)\,[(1/S^2) - P_i^2]} \quad (2)$$

where $N = N_r + N_l$. Since $P_i \leqq 1$ and $S \lesssim 0.3$ for general polarization detectors, $1/S^2 >> P_i^2$, so that Eq. (2) becomes:

$$\delta P_i = 1 / \sqrt{S^2 N} \quad (3)$$

If N_0 electrons are needed to enter the Mott apparatus for detecting N scattered electrons, Eq. (3) becomes:

$$\delta P_i = 1 / \sqrt{\gamma S^2 N_0} \quad (4)$$

where

$$\gamma = N/N_0 \quad (5)$$

Eq. (4) indicates that the statistical error δP_i becomes smaller as γS^2 increases. Thus, γS^2 quantitatively represents the efficiency of the polarization detector. This value can be written as:

$$F = \gamma S^2 \quad (6)$$

and is used as a figure of merit for the Mott detector (Kessler, 1976).

For distinguishing two different areas in an image, the next relationship must be satisfied:

$$\Delta S_g / N_s \gtrsim C \quad (7)$$

Here ΔS_g is the difference between image signals obtained from two different areas, N_s is the noise and C is a predefined constant. In a spin-polarized SEM, the image signal is represented by polarization P_i, so that $\Delta S_g = \Delta P_i$. In addition, the predominant noise is statistical noise, so that $N_s = \delta P_i$. Accordingly, Eq. (7) becomes:

$$\Delta P_i / \delta P_i \gtrsim C. \quad (8)$$

N_0 in Eq. (4) can be expressed using probe current I_p as:

$$N_0 = t_0 \gamma_t \gamma_s I_p / e \quad (9)$$

In this equation t_0 is the time necessary for making one pixel, γ_t is a transfer function of secondary electrons from a sample to the Mott detector, γ_s is the yield of secondary electrons, and e is the electronic charge. From Eqs. (4), (6), (8), and (9), it follows that:

$$P_i \sqrt{F t_0 \gamma_t \gamma_s I_p / e} > C \quad (10)$$

For the present study, $F = 6 \times 10^{-6}$, $\gamma_t \gamma_s = 0.4$ (measured at a primary electron energy of 4 keV for the cobalt sample), $t_0 = 10$msec, and $e = 1.6 \times 10^{-19}$ Coulomb. Furthermore, if $C = 5$ (Rose, 1948), Eq. (10) becomes:

$$I_p > 2 \times 10^{-10} (\Delta P_i)^{-2} \quad (11)$$

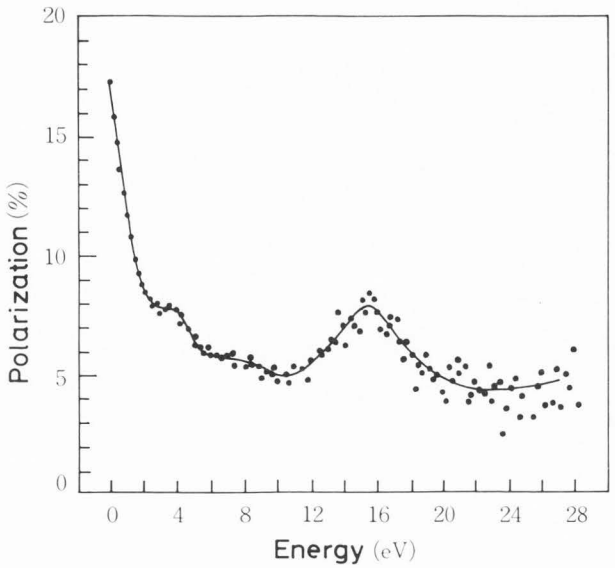

Fig. 1. Spin polarization of the secondary electrons from Ni(110) as a function of energy.

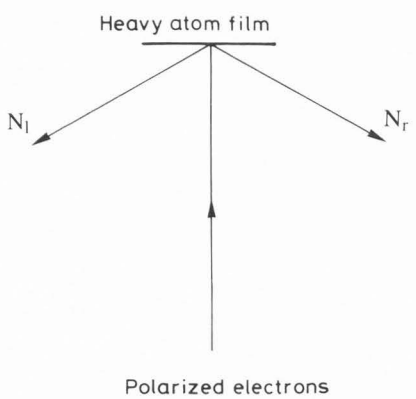

Fig. 2. Principle of Mott detector.

According to experiment, when two domains have opposite magnetization directions, $\Delta P_i = 0.5$ for iron. As a result, a probe current larger than 0.8nA is needed in order to distinguish the domains, as given by Eq. (11). This value is about one hundred times larger than that for an ordinary SEM.

For achieving a sufficiently fine probe beam, despite this larger probe current, a field emission (FE) gun is suitable because of its high brightness (Koike et al., 1985a). A schematic diagram of this FE gun is shown in Figure 4 (Todokoro et al., 1981). A relatively long working distance of 45mm enables the secondary electron collector to be mounted near the sample. The calculated relationship between probe diameter and probe current is shown in Figure 5. In this calculation, spherical, chromatic, and diffraction aberrations of only magnetic lens are taken into account, because Butler-type anode aberration is negligibly small for the operational voltage. It is assumed that the FE-source diameter is 3nm, energy spread is 0.3eV, and emission current is 100 μA/steradian.

To satisfy the condition of Eq. (11), an aperture diameter of 0.15mm was selected. In this case, probe diameters of 22 and 35nm are expected for energies of 10 and 4 keV, respectively, both with probe currents of 3nA.

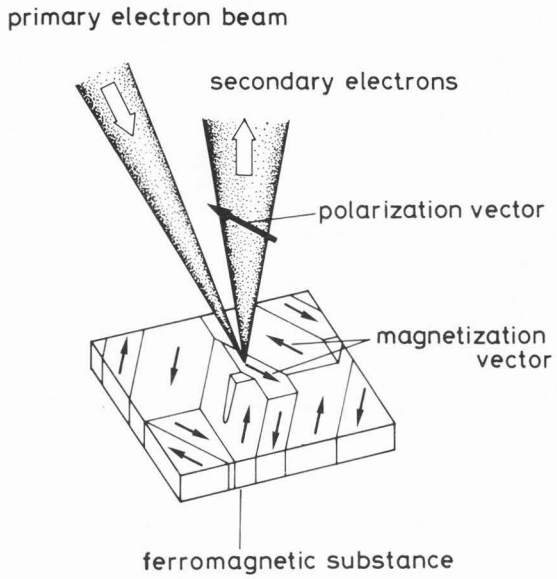

Fig. 3. Principles of magnetic domain observation.

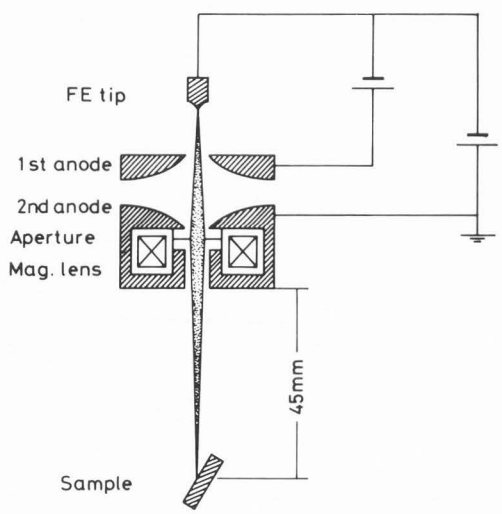

Fig. 4. Schematic diagram of field emission gun.

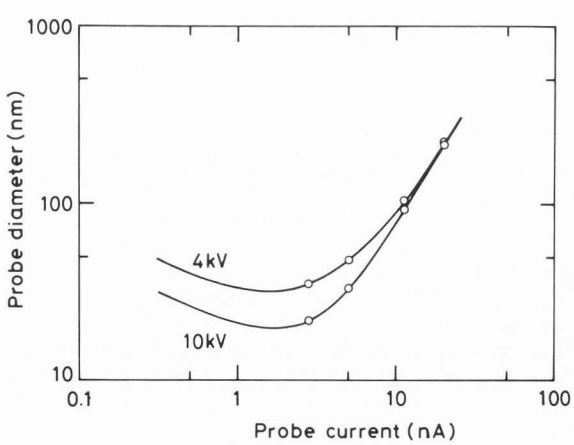

Fig. 5. Dependence of probe diameter on probe current.

Magnetic Contrast Independent of Surface Morphology

Magnetic domain images obtained using conventional methods are usually superimposed magnetic and surface morphological contrasts. This is because, in conventional methods, the intensity of light or electron beams are used as an image signal, which represents not only magnetization but also surface morphology. In spin-polarized scanning electron microscopy, the polarization of secondary electrons is used as an image signal. From Eq. (1), this polarization is the value of $(N_l - N_r)$ normalized by $(N_l + N_r) = N$. Since N is proportional to the secondary electron intensity, polarization is independent of this intensity, so that the surface morphological contrast should not appear.

Simplified Relationship between Image Signal and Magnetization, and the Detection of Magnetization Direction

When one polarization vector component P_i is used as an image signal, P_i can be expressed by:

$$P_i = P\cos\phi \tag{12}$$

Here, P is the absolute value of polarization vector **P**, and ϕ is the angle between **P** and the polarization detection direction. As mentioned before, **P** is related to magnetization vector **M**, expressed by:

$$\mathbf{P} \propto \mathbf{M} \tag{13}$$

From Eqs. (12) and (13):

$$P_i \propto M\cos\phi \tag{14}$$

where M is the absolute value of **M**. Eq. (14) shows that the relationship between the image signal obtained from this method and magnetization is much simpler and more quantitatively reliable than in conventional SEM methods (Jones 1976, Shimizu et al. 1976).

It is possible to detect three polarization vector components; one way is shown in Figure 6. By using two pairs of electron detectors, (D_1, D_2) and (D_3, D_4), P_x and P_y can be detected respectively. P_z can also be detected when the polarization vector is rotated by 90° around the y axis in a spin rotator, and a pair of detectors, (D_1, D_2) is used. From these three polarization vector components, the direction of the polarization vector, (i.e., magnetization vector direction) can be determined.

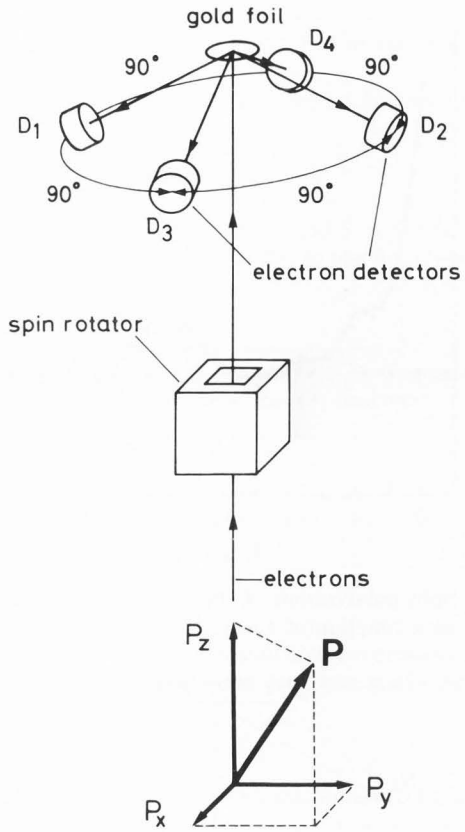

Fig. 6. Principle of detecting three polarization vector components.

Experimental

A schematic diagram of a spin-polarized SEM is shown in Figure 7. It mainly consists of an ordinary SEM equipped with an FE gun, and Mott detector for spin analysis. The FE gun can be operated with an acceleration voltage of up to 10 kV and probe current of up to 100 nA, depending on the probe diameter as shown in Fig. 5. Secondary electrons from a sample surface are collected with an extraction lens and transferred to the Mott detector. In this detector, these electrons accelerate up to 100 keV and strike a 50 nm thick gold foil target. The electrons scattered by this target at an angle of 120° ±8° are detected by four surface barrier detectors (SBDs) located at four fold symmetrical positions about the incident beam, to simultaneously detect two polarization vector components.

The samples used in this study were single-crystal iron-1.5% silicon (001), cobalt $(1\bar{2}10)$, and polycrystal iron. The single-crystal samples were 1 mm thick and the polycrystal one was

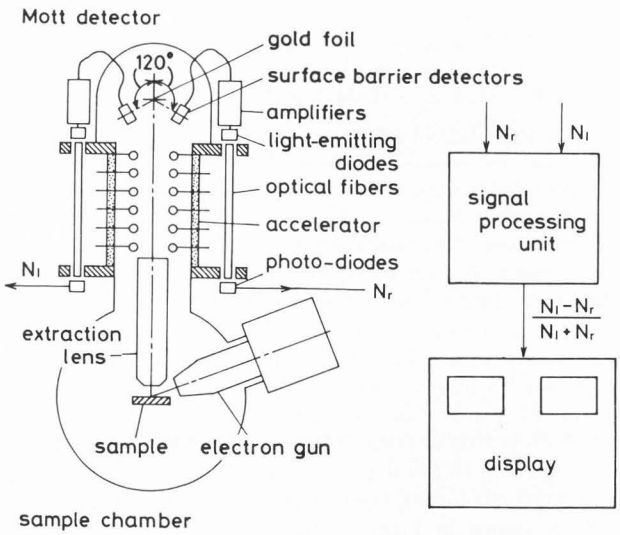

Fig. 7. Schematic diagram of spin-polarized SEM.

0.5 mm thick; all samples had surface areas of approximately 1 cm^2. The samples were mechanically polished, electropolished (cobalt sample only), and annealed in a vacuum at about 800° ~ 900°C for 20 min. They were then cleaned for 20 min using approximately 15μA argon ion bombardment at 2 keV.

It took 10 min to form a complete domain image. To obtain one pixel, 10 ms were required. During this period, 2.5×10^3 electrons were typically detected in the Mott detector.

Magnetic Domain Observation and Discussions

Magnetic contrast obtained from iron and cobalt

The domain images of the cobalt $(1\bar{2}10)$ and iron-1.5% silicon (001) surfaces, with arrows indicating the magnetization directions, are shown in Figures 8(a) and (b) (Koike et al., 1985b). In these pictures, the image signals were obtained from the polarization vector component P_i along the arrow shown at the top left of the figure. The crystals were set so that one of the magnetization easy axes (⟨0001⟩ for cobalt and ⟨001⟩ for iron) was amost parallel to the polarization detection direction. The magnetization direction in each domain was determined by taking into account the sign of P_i, the direction of the magnetization easy axes, and conservation of the normal magnetization vector components at the domain boundaries. P_i for the white areas in Figs. 8(a) and (b) was 18% and 25%, respectively. Since the magnetization in these areas is almost parallel to the polarization detection direction, these values represent the magnitude P of the polarization vector.

Spatial resolution

To check the spatial resolution, the iron polycrystal with an average grain size of about 100μm was observed, which was expected to have a small domain size. The domain images of the iron polycrystal surface are shown in Figures 9(a) and (b). In addition, the absorption current images of the same respective areas are shown in Figures 9(c) and (d) (Koike et al., 1985c). The upper left-hand portions of the areas in (a) and (c) are magnified ten times to give (b) and (d), respectively.

In Figure 9(d), a black streak whose minimum width is 0.1μm can be identified. Thus, the probe beam diameter is thought to be less than 0.1μm. In Fig. 9(b), two domains (white and black) can be distinguished, where the centers are 0.2μm apart. As a result, the spatial resolution of this SEM is 0.2μm for an iron sample.

Domain contrast and surface morphology

The domain image of the cobalt $(1\bar{2}10)$ surface and the absorption current image of the same area are shown in Figures 10(a) and (b), respectively (Koike et al., 1985b). In Fig. 10(b), the streaks running from the top left to bottom right are thought to be scratches made during polishing. From these figures, it can be seen that domain image (a) does not show any of the topographical contrast seen in Fig. 10(b). Thus, the domain contrast obtained with a spin-polarized SEM is independent of the topographical contrast. Sometimes, surface topography can affect the domain structure. If necessary, the relationship can be studied by comparing these two kinds of pictures. For example, the scratches seen on the left-hand side of Fig. 10(b) generate the fine domains seen in the same area of Fig. 10(a). However, the scratches seen on the right-hand side of Fig. 10(b) appear to have no effect on the domain structure. This could occur if the scratches on the left were deeper than those on the right.

A domain image of the iron polycrystal surface and an absorption current image of the same area are shown in Figures 11(a) and (b) (Koike et al., 1985b), respectively. Here, it can be seen that domain image (a) does not show any grain contrast or contrast due to crystallographic orientation as seen in Fig. 11(b). Thus the domain contrast is also independent of grain contrast. The relationship between domain and grain can be investigated. The grains labeled a, b and c in Fig. 11(b) have larger domains, whereas those labeled e, f and g have finer domains. Thus, it is thought that the magnetization easy axis of the former grains lies near the sample surface, while that of the latter grains lie at some angle to the sample surface.

Magnetic Contrast and Magnetization Direction

To check the relationship given by Eq. (14), a cobalt $(1\bar{2}10)$ surface has been observed during sample rotation. Since the cobalt has only one magnetization easy axis, ⟨0001⟩, it has stripe domains where the magnetization is parallel or antiparallel to [0001]. Thus, if the sample is rotated around the axis perpendicular to the sample surface, the magnetic contrast should change according to Eq. (14).

The results are shown in Figure 12 (Koike and Hayakawa, 1985). The angle between the polarization detection direction and the crystal axis of [0001] is represented by ϕ. The image contrast is a maximum at $\phi = 0°$, decreases with increasing ϕ when $90° > \phi > 0°$, disappears at $\phi = 90°$, and then increases with ϕ but in reversed contrast. Therefore this series of images confirms that the image contrast can be expressed by Eq. (14).

The domain images of the iron-1.5% silicon (001) are shown in Figure 13 (Koike et al., 1985b). Part of the area in Fig. 13(a) is magnified and represented in Fig. 13(b), with arrows indicating the magnetization directions. In this case, the [100] axis (one of the magnetization easy axes of the sample) differs from the polarization detection direction by 16°. It is possible for the magnetic domains of this surface to have four different magnetization directions. P_i for these domains is 24, 7, −7, and −24%, corresponding to white, light gray, dark gray, and black, respectively, in Fig. 13. As a result, the magnetization direction in each domain is determined as indicated in Fig. 13(b).

The domain images of an iron polycrystal surface obtained from different image signals (i.e., polarization vector components orthogonal to each other) are shown in Figures 14(a) and (b), respectively. Furthermore, an absorption current image is shown in Figure 14(c). All figures are obtained from the same area on the sample.

From Figs. 14(a) and (b), which seem to be dissimilar, the directions of the magnetization vector components in the sample surface can be determined. An example of this is shown in Figure 15. Part of the domain images surrounded by rectangles in Figs. 14(a) and (b) are reproduced in schematic form and shown in Figs. 15(a) and (b) respectively. The arrows in these domain images indicate magnetization vector components along the polarization detection direction of the respective image. By composing two magnetization vector components at corresponding points in Figs. 15(a) and (b), the magnetization vector components on the sample surface are determined as shown in Fig. 15(c).

Prospect of Spin-Polarized SEM

Magnetic recording density is rapidly increasing and minimum bit length of recording is heading into the sub-micron region. Conventional methods for a thick sample are no longer suitable for the study of the magnetic states of recorded materials, because of their poor spatial resolution. In this context, the use of spin-polarized SEMs will be valuable for this purpose.

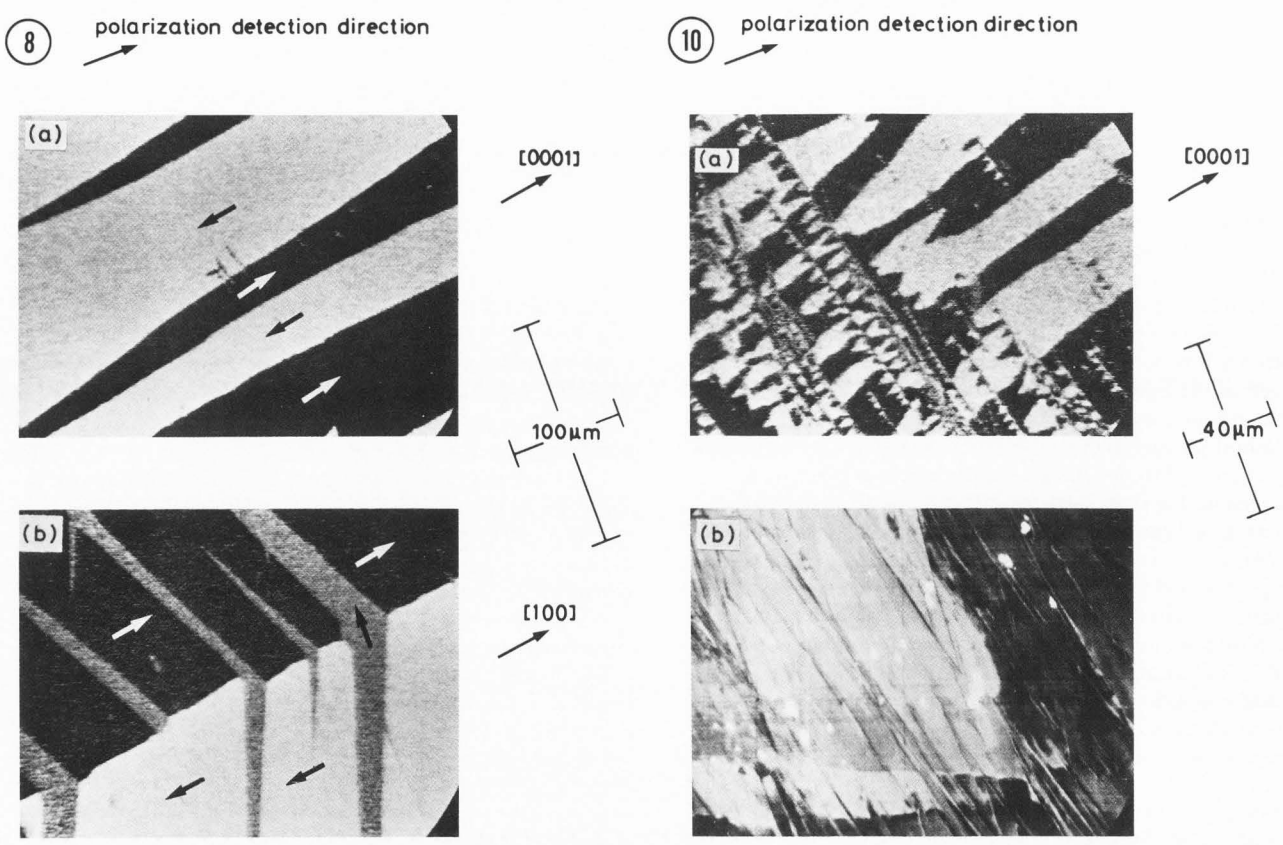
8
polarization detection direction
(a)
[0001]
100μm
(b)
[100]
10
polarization detection direction
(a)
[0001]
40μm
(b)

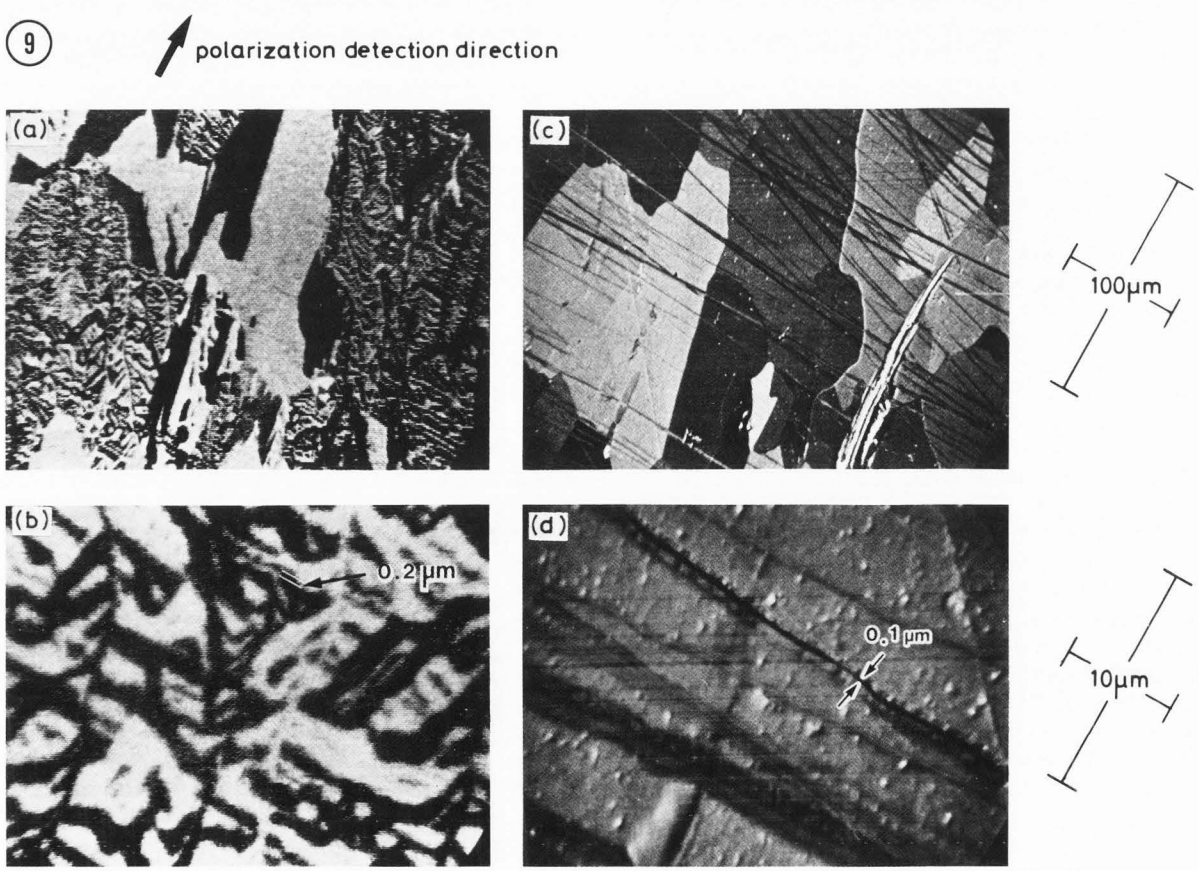
9
polarization detection direction
(a)
(c)
100μm
(b)
0.2μm
(d)
0.1μm
10μm

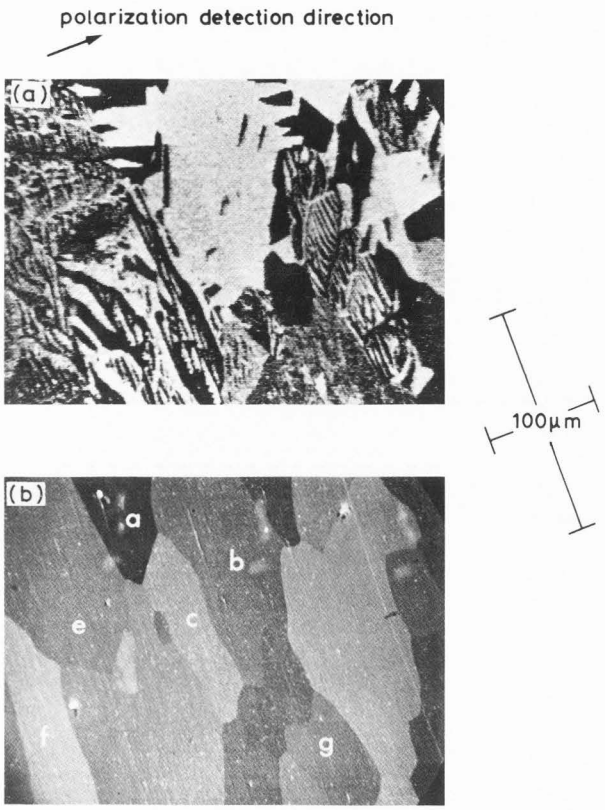

Fig. 11. (a) Domain image of iron polycrystal surface and (b) absorption current image of area shown in (a).

The Mott detector used for spin analysis in the spin-polarized SEM is extremely bulky compared with an electron detector used in a conventional SEM. Recently, new attempts to use different types of spin analyzers in spin-polarized SEM have been made independently by Kirschner (1985) and Unguris et al. (1986). Both of these analyzers are operated at a low voltage around 100 V and are very compact. Such compact spin-analyzers will promote the spread of this new domain observation method.

Conclusions

In this paper spin-polarized scanning electron microscopy for magnetic domain observation has been reviewed. This is a unique method where spin polarization of secondary electrons is used to form images instead of the secondary electron number as in conventional SEM. This method has additional capabilities, such as magnetic contrast independent of surface morphology, magnetization direction detection, and high spatial resolution. Considering all of these advantages, this SEM is a very promising tool for the study of magnetic materials.

Fig. 8. Domain image of (a) cobalt ($1\bar{2}10$), and (b) iron-1.5% silicon (001) surface. Arrows in the photographs indicate magnetization direction.

Fig. 9. Domain images (a,b) and absorption current images (c,d) of an iron polycrystal. Images (a,b) are obtained from the same areas as (c,d) respectively. Sections of the areas in (a,c) are magnified ten times in (b,d).

Fig. 10. (a) Domain image of cobalt ($1\bar{2}10$) surface, and (b) absorption current image of area shown in (a).

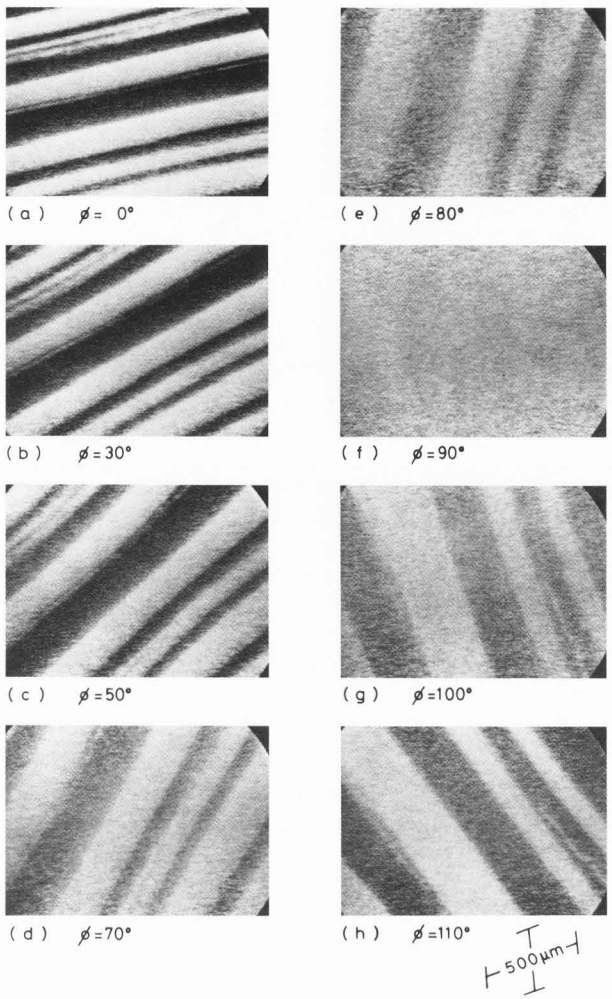

Fig. 12. Series of domain images of a cobalt ($1\bar{2}10$) surface as the sample was rotated around the axis perpendicular to the sample surface; ϕ indicates the rotation angle.

Acknowledgements

The authors would like to thank Dr. M. Ichikawa and S. Kawase for their helpful suggestions concerning the use of the FE gun, and Dr. A. Fukuhara and Dr. S. Harada for their valuable advice and encouragement during the course of this study.

References

Chrobok G, Hofmann G. (1976). Electron spin polarization of secondary electrons ejected from magnetized europium oxide. Phys. Lett. **57A**, 257–258.

DiStefano TH. (1978). Technology for detecting small magnetic domains and beam-addressed memory therewith. IBM Tech. Discl. Bull. **20**, 4212–4215.

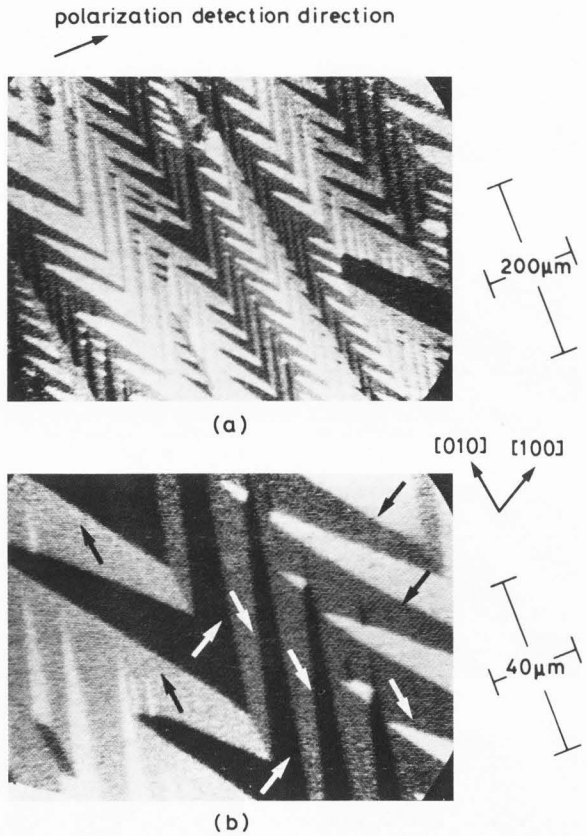

Fig. 13. Domain images of iron-1.5% silicon (001) surface. A section of the area in (a) is magnified in (b). The [001] axis differs from the polarization detection direction by 16°.

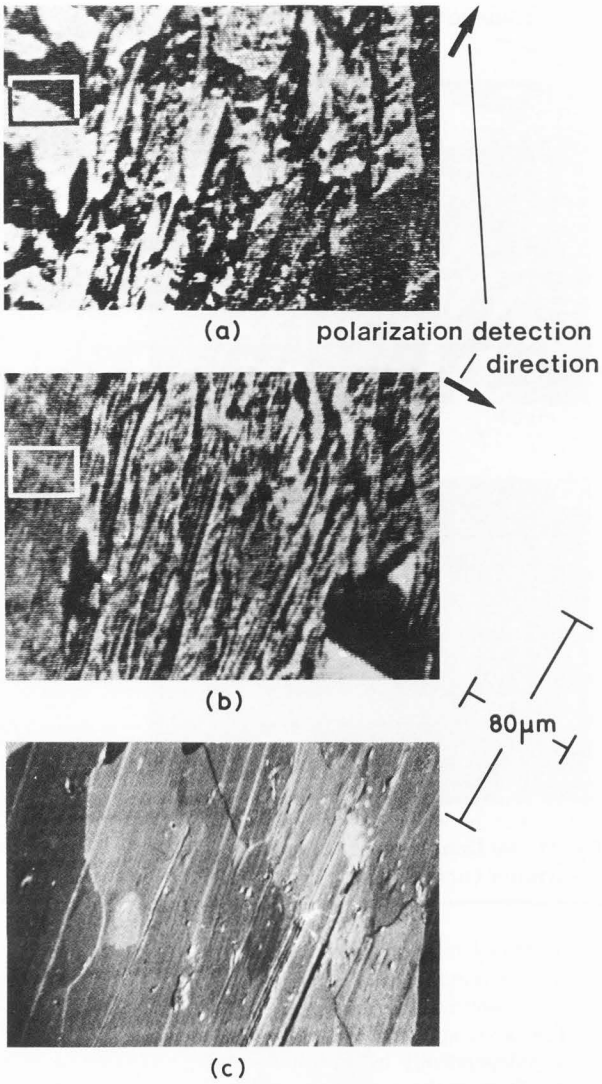

Fig. 14. (a,b) Domain images of an iron polycrystal surface obtained from polarization vector components orthogonal to each other, and (c) absorption current image of area shown in (a,b).

Hopster H, Raue R, Kisker E, Güntherodt G, Campagna M. (1983). Evidence for spin-dependent electron-hole pair excitations in spin-polarized secondary-electron emission from Ni(110). Phys. Rev. Lett. **50**, 70–73.

Jones GA. (1976). On the quality of Type I magnetic contrast obtained in the scanning electron microscope. Phys. Stat. Sol. (a)**36**, 647–657.

Kessler J. (1976). Polarized electrons. Springer-Verlag (Berlin, Heidelberg, New York), 79.

Kirschner J. (1984). On the role of the electron spin in scanning electron microscopy. Scanning Electron Microscopy 1984; III: 1179–1185.

Kirschner J. (1985). Magnetic-structure analysis in scanning electron beam devices by means of the LEED spin-polarization detector. Appl. Phys. **A36**, 121–123.

Kirschner J, Feder R. (1979). Spin polarization in double diffraction of low-energy electrons from W(001): experiment and theory. Phys. Rev. Lett. **42**, 1008–1011.

Kisker E, Gudat W, Schröder K. (1982). Observation of a high spin polarization of secondary electrons from single crystal Fe and Co. Solid State Commun. **44**, 591–595.

Koike K, Hayakawa K. (1984a). Scanning electron microscope observation of magnetic domains using spin-polarized secondary electrons. Jpn. J. Appl. Phys. **23**, L187–L188.

Koike K, Hayakawa K. (1984b). Observation of magnetic domains with spin-polarized secondary electrons. Appl. Phys. Lett. **45**, 585–586.

Koike K, Hayakawa K. (1985). Domain observation with spin-polarized secondary electrons. J. Appl. Phys. **57**, 4244–4248.

Koike K, Matsuyama H, Todokoro H, Hayakawa K. (1985a). Spin-polarized scanning electron microscope for magnetic domain observation. Jpn. J. Appl. Phys. **24**, L542–L544.

Koike K, Matsuyama H, Todokoro H, Hayakawa K. (1985b). Spin-polarized scanning electron microscopy. Jpn. J. Appl. Phys. **24**, 1078–1081.

Koike K, Matsuyama H, Todokoro H, Hayakawa K. (1985c). High spatial resolution spin-polarized scanning electron microscope. Jpn. J. Appl. Phys. **24**, L833–L834.

Penn DR, Apell SP, Girvin SM. (1985a). Theory of spin-polarized secondary electrons in transition metals. Phys. Rev. Lett. **55**, 518–521.

Penn DR, Apell SP, Girvin SM. (1985b). Spin polarization of secondary electrons in transition metals: Theory. Phys Rev. **B32**, 7753–7768.

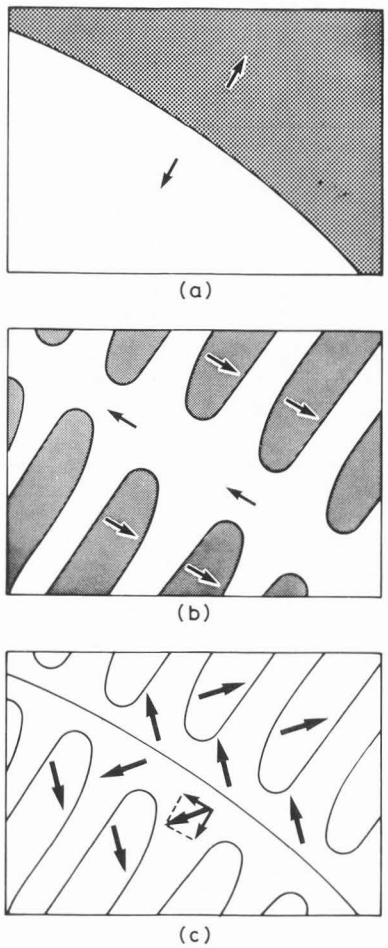

Fig. 15. (a,b) Sketches of sections of areas shown in Fig. 14 (a,b) respectively, and (c) directions of magnetization vector components on the sample surface.

Rose A. (1948). Television pickup tubes and the problem of vision. Adv. Electron. **1**, 131–166.

Shimizu R, Ikuta T, Kinoshita M, Murayama T, Nishizawa H, Yamamoto T. (1976). High contrast observation of magnetic domain with high voltage SEM. Jpn. J. Appl. Phys. **15**, 967–981.

Siegmann HC, Pierce DT, Cellota RJ. (1981). Spin-dependent absorption of electrons in a ferromagnetic metal. Phys. Rev. Lett. **46**, 452–455.

Todokoro H, Sakitani Y, Fukuhara S, Okajima Y. (1981). Development of a scanning electron microscope equipped with a field emission gun. J. Electron Microsc. **30**, 107–113.

Unguris J, Pierce DT, Galejs A, Celotta RJ. (1982). Spin and energy analyzed secondary electron emission from a ferromagnet. Phys. Rev. Lett. **49**, 72–76.

Unguris J, Hembree G, Celotta RJ, Pierce DT. (1986). Investigations of magnetic microstructures using scanning electron microscopy with spin polarization analysis. J. Magnetism Magnetic Mater. **54–57**, 1629–1630.

Discussion with Reviewers

J. Kirschner: You point out clearly that at the present time the practical magnetic resolution is given by considerations of signal-to-noise and measurement time for a full frame. However, the ultimate resolution may be much better than the 200 nm demonstrated in Fig. 9. What is the resolution you obtain in e.g., a line scan across a domain wall?

Authors: We estimated the magnetic resolution from the minimum distance between the centers of two domains which can be distinguished. We think, if sufficiently fine domain structure exists in an observed area, this value is almost equal to the blurred width of a domain wall and to electron probe diameter. We took a number of pictures to confirm the best resolution. However, we had no way of knowing if there is a sufficiently small domain in the observed area or not, and if not, we could not confirm the resolution less than the minimum domain size, even if our SEM has the potential for higher resolution. Thus, some possibility still remains that the resolution is better than 200 nm. Another method known to check spatial resolution is to measure blurred domain wall width. If this method is applied to Fig. 9, spatial resolution is found to be less than 100 nm. However, we did not use this value as the resolution of our SEM. The reason is that the blurred domain width seemed to be reduced by increasing image contrast photographically, and thus this method is not sufficient to convince readers of the resolution of our SEM.

J. Unguris: The highest spatial resolution in a polarization image shown in this paper is about 200 nm. Why is this so much larger than the expected electron probe diameter of 30 nm and do the authors expect to eventually achieve the higher resolution?

Authors: We used the same electron gun as used by Todokoro et al. (1981) with almost the same operating conditions. They achieved spatial resolution of 20 nm. Thus, we think there is no essential difficulty to achieve resolution around 30 nm in our SEM. There are three possible reasons why calculated resolution is not achieved at present. One is mechanical vibration of the apparatus. Another is misalignment of the electron optical system. The final reason is, as mentioned above, the sample used here did not have a domain small enough to check for best resolution.

H.C. Siegmann: In the section of "High Spatial Resolution," the statement is made that 100 times larger current is needed for the polarization microscope compared to an ordinary SEM. What type of contrast is referred to by this statement?

Authors: We are referring to topographical contrast for an ordinary SEM in which secondary electron intensity is used as an image signal.

H.C. Siegmann: How is the vacuum condition and deterioration of contrast with time?

Authors: The vacuum pressure in the sample chamber is about 2×10^{-9} Torr. Even after leaving a clean iron single crystal surface in a residual gas of 5×10^{-7} Torr for about a month, we could still observe a domain image but with much reduced contrast.